ADVANCES IN ATMOSPHERIC SCIENCES, VOL. 36, DECEMBER 2019, 1371–1380

• **Original Paper** •

On the Interrelation between Spring Bihemispheric Circulations at Middle and High Latitudes

Chuhan LU* and Zhaoyong GUAN

Key Laboratory of Meteorological Disaster, Ministry of Education/Collaborative Innovation Center on Forecast and Evaluation of Meteorological Disasters, Nanjing University of Information Science and Technology, Nanjing 210044, *China*

(Received 9 March 2019; revised 30 June 2019; accepted 8 August 2019)

ABSTRACT

Bihemispheric atmospheric interaction and teleconnection allow us to deepen our understanding of large-scale climate and weather variability. This study uses 1979–2017 spring NCEP reanalysis to show that there is interrelation between bihemispheric circulations at the extratropics. This is regarded as a significant negative correlation between the Antarctic and the Arctic regional surface air pressure anomalies, which is induced by interhemispheric oscillation (IHO) of the atmospheric mass. The spatial pattern of IHO is characterized by antiphase extratropical airmass anomalies and geopotential height anomalies from the troposphere to stratosphere between the Southern and Northern Hemisphere. IHO is closely related to stronger bihemispheric low-frequency signals such as Antarctic Oscillation and Arctic Oscillation, thereby demonstrating that IHO can be interpreted as a tie in linking these two dominant extratropical circulations of both hemispheres. IHO is associated with a strong meridional teleconnection in zonal winds from the middle–high troposphere to the lower stratosphere, with the wind anomalies in the form of alternate positive–negative wavy bands extending from the Antarctic to Arctic region, which act as a possible approach to interactions between the bihemispheric atmospheric mass. It is argued that IHO-related omega angular momentum anomalies led by the extratropical atmosphere cause the meridional teleconnection of relative angular momenta, thereby giving rise to the zonal wind anomalies. The modeling of GFDL and UKMO as components of the CMIP5 project have been verified, achieving the related IHO structure shown in the present paper.

Key words: bihemispheric interaction, extratropical atmosphere, interhemispheric oscillation

Citation: Lu, C. H. and Z. Y. Guan, 2019: On the interrelation between spring bihemispheric circulations at middle and high latitudes. *Adv. Atmos. Sci.*, **36**(12), 1371–1380, https://doi.org/10.1007/s00376-019-9047-4.

Article Highlights:

- A strong antiphase relationships of surface air pressure anomalies presents between the Antarctic and the Arctic in boreal spring.
- IHO closely links with the antiphase extratropical circulations between the NH and the SH.
- The IHO-associated relative and omega angular momentum anomalies can maintain the interhemspheric teleconnection of circulation.

1. Introduction

Interhemispheric atmospheric interaction and teleconnection are of considerable interest because of the insight such relationships provide toward understanding climate and weather variability. The thought that perhaps there is physical interaction between the hemispheres dates back to at least the correlation studies of Walker (1924), which showed patterns of global-scale coherence in the pressure field that later have been associated with the Southern Oscillation phenomena. Studies of interhemispheric interactions have shown that there is a relationship between rainfall and temperature over South America and the Southern Oscillation (Namias, 1963; Trenberth, 1976). The spatial coherence of African rainfall anomalies (Nicholson and Entekhabi, 1986) was also shown to be related to interhemispheric exchange of the atmospheric angular momentum (Newell et al., 1969).

The conservation of global air mass requires that any "gain" in air mass in one hemisphere must be balanced by a "loss" of air mass in the other. For example, when the winter hemisphere experiences an increase in average pres-

* Corresponding author: Chuhan LU
Email: luchuhan@nuist.edu.cn

sure due to cooling, the summer hemisphere experiences a decrease in average pressure (Chen et al., 1997). Antiphase changes in air pressure can lead to detectable deformations at Earth's surface (Blewitt et al., 2001). Analysis of the daily surface air pressure (SAP) demonstrates that exchanges of air mass occur between hemispheres across the equator (Baldwin, 2001). The phenomenon of atmospheric blocking was observed in 1979 over the Southern Pacific Ocean, at the same time as an increase in sea level pressure (SLP) of 1 hPa (Christy et al., 1989). Christy et al. (1989) illustrated how cross-equatorial atmospheric mass fluxes can lead to significant localized climatic anomalies. Whenever there is a substantial loss of dry atmospheric mass from the Northern Hemisphere (NH), increases in pressure in Southeast Asia may lead to enhanced surface ridging over the southern Pacific and southern Indian oceans. It is interesting to note that these are regions in which atmospheric blocking regularly occurs (Carrera and Gyakum, 2003).

To date, research in interhemispheric interaction and exchange has focused on the interaction between the tropical region and other regions, by considering cross-equatorial atmospheric mass fluxes. Extratropical-to-extratropical teleconnection between the NH and the Southern Hemisphere (SH) has yet to be studied in detail. Guan and Yamagata (2001) introduced the idea of interhemispheric oscillation (IHO) in the SAP field to describe comparable but opposite changes of air mass between hemispheres. Time series of the IHO index with a wide range of spectra from a few months to decades indicate atmospheric mass redistribution resulting from mass exchange between the hemispheres. Guan et al. (2010) and Lu et al. (2008) described how the interannual variability of the IHO at mid and high latitudes causes variations in global atmospheric circulation.

During boreal spring, there is a significant exchange of atmospheric mass (Chen et al., 1997). In view of the distribution showing that spring IHO-caused air mass anomalies are mainly at the extratropics (Lu and Guan, 2009), the pattern is likely to be connected with the stronger low-frequency signals such as Antarctic Oscillation (AAO), which is a dominant atmospheric oscillation in the middle and high southern latitudes (Gong and Wang, 1999), and Arctic Oscillation (AO), the leading mode of low-frequency variability in the mid–high northern latitudes (Thompson and Wallace, 1998). However, the relationship between airmass anomalies over hemispheric high latitudes and its possible pathway remain unclear. Potential connections or contributions of IHO to the connection of air mass between hemispheric high latitudes and how this unbalanced hemispheric air mass maintains should be discussed, which is the motivation of this study. More specifically, our aim is to investigate the possible connection between bihemispheric extratropical atmospheric circulation and attempt to link this with IHO. We then describe how IHO is established by wind-field transport and atmospheric angular momentum.

The remainder of the paper is organized as follows. In section 2, we describe our sources of data and methods of analysis. We describe the link between bihemispheric extratropical atmospheric circulations and IHO in section 3, as well as discuss the relationship between IHO and atmospheric angular momentum. In section 4, we examine the GFDL and UKMO model results from CMIP5 to assess the robustness of the IHO pattern. Finally, in section 5, we draw some conclusions and suggest avenues of further research.

2. Data and methods

2.1. *Data*

The data used consist of NCEP1 monthly reanalysis (Kalnay et al., 1996), including geopotential height, zonal wind, and SAP at the resolution of 2.5° latitude × 2.5° longitude and covering the spring (the mean over March to May each year) for 1979–2017. Additionally, the r1i1p1 modeling outputs from GFDL-CM3 and HadCM3 submitted to the CMIP5 project are used to verify the results from reanalysis in 27 spring seasons for 1979–2005. The vertical levels of GFDL are roughly in agreement with NCEP data, except that HadCM3 is reduced by 10 hPa.

2.2. *Methods*

2.2.1. *IHO index construction*

Differing from the SLP over a terrain area artificially corrected to sea level height pressure, the SAP is the atmospheric pressure above the surface of Earth, which can represent Earth's surface air mass more accurately. Hence, the interannual variability of SAP under discussion actually denotes the corresponding condition of atmospheric mass over Earth. Remarkably, anticorrelative evolution is found in the time-dependent hemispheric mean surface pressure anomalies in spring (Fig. 1), with a correlation coefficient of −0.771. Because of the smaller interannual variability of water vapor, dry air masses play a key role in the interannual variation of airmass redistribution (Lu et al., 2008). Due to global dry air conservation, this significant anticorrelation feature demonstrates that interhemispheric atmospheric air masses balance well between the NH and SH. That is, the bihemispherical surface pressure difference can be the measure-

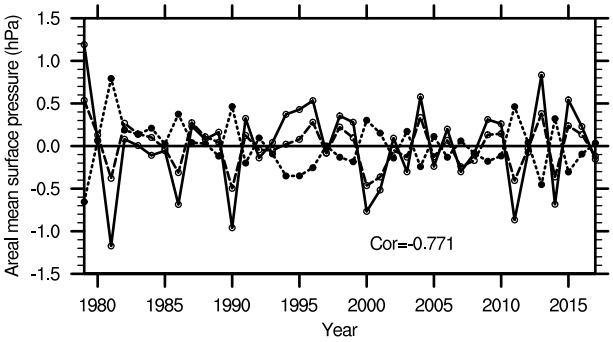

Fig. 1. Area-averaged time-dependent spring SAP anomalies in the SH (dotted line) and NH (dashed line) and IHO index (solid line), in hPa. The correlation coefficient (Cor) between the time series of the area-average SAP in the SH and the NH one is −0.771.

ment for the strength of interhemispheric air exchange and interactions. According to Guan and Yamagata (2001), the SAP is utilized to construct spring monthly IHO by means of the following equations:

$$I_{\mathrm{IHO}} = p_{\mathrm{s,NH}} - p_{\mathrm{s,SH}}$$
$$p_{\mathrm{s,NH}} = \int_0^{\pi/2} \overline{p_{\mathrm{s}}} \cos\varphi \mathrm{d}\varphi \,, \tag{1}$$

where $p_{\mathrm{s,NH}}$ and $p_{\mathrm{s,SH}}$ denote the area-averaged surface pressure anomalies over the NH and SH respectively, φ denotes the latitude, and $\overline{p_{\mathrm{s}}}$ denotes the zonal mean values of SAP anomalies.

2.2.2. *AAO and AO index construction on pressure levels*

By examining the association of IHO with AAO and AO at all pressure levels, we aim to reveal the interhemispheric interactions, especially at the extratropics. Thus, referring to Baldwin and Thompson (2009), we use EOF analysis of anomalous zonal mean heights on all 17 levels (1000–10 hPa) in 20°–90°S and 20°–90°N, arriving at the corresponding temporal coefficients of the first mode of EOF as the leveled AAO and AO indices. The AAO and AO sequences thereby constructed are indicative of their variations in each layer (Baldwin and Thompson, 2009).

2.2.3. *Atmospheric angular momentum*

From the point of view of global angular momentum, we speculate that the maintenance mechanism for the large-scale redistribution of air mass may be the corresponding change in angular momentum. Following von Storch (2000), we have the equations of the hydrostatic approximation of relative angular momentum (m_{r}) and omega angular momentum (m_{Ω}), as given below:

$$\begin{cases} m_{\mathrm{r}}(\varphi) = \dfrac{2\pi r^2}{g} \displaystyle\int_{10}^{p_{\mathrm{s}}} r\cos\varphi \overline{u} \cos\varphi \mathrm{d}p\mathrm{d}\varphi \,, \\ m_{\Omega}(\varphi) = \dfrac{2\pi r^2 \Omega}{g} (r\cos\varphi)^2 \overline{p_{\mathrm{s}}} \cos\varphi \mathrm{d}\varphi \,, \end{cases} \tag{2}$$

where Ω represents the angular velocity of Earth, r the radius of earth, u the zonal wind and p the pressure. Vertical integration is conducted from the surface to 10 hPa using 10 hPa as the top level of the NCEP data.

3. Link between interhemispheric air at the extratropics and IHO

3.1. *Surface pressure anomalies and 850-hPa wind anomalies*

To find the interrelationship between the extratropical atmospheres of both hemispheres, we calculated the departures of spring areal mean surface pressure at 60°–90°N and 60°–90°S from 1979 to 2017 (Fig. 2a). The variations in high-latitude mean surface pressure are comparable, but with opposite sign in both of the hemispheres. The correlation coefficient reaches −0.304 at the significance level of 0.06 based on the *t*-test. This indicates that the air mass distributes in a seesaw pattern between the hemispheres during the spring season. Nevertheless, there is no such clear relationship between 0°–60°N and 60°–90°S, with a correlation coefficient of 0.02 (figure not shown). This fact shows that the interhemispheric surface pressure oscillation exhibits the inter-association of varying atmospheric mass mainly at bihemispheric extratropics. As documented in Table 1, the anticorrelation of regional mean SAP anomalies between the northern high latitudes ($\mathrm{NH_h}$) and the southern ones ($\mathrm{SH_h}$) is indeed most significant in boreal spring compared to other seasons. Furthermore, the correlation coefficient between IHO and both $\mathrm{NH_h}$ and $\mathrm{SH_h}$ in spring is 0.61 and −0.62 respectively, with the highest significance (> 0.01) among all the four seasons. Thus, IHO shows notable seasonality, which is consistent with Guan et al. (2010). In particular, the spring IHO links closely with the interhemispheric unbalance and connection of air mass, and is especially pronounced over high latitudes.

IHO-associated surface pressure shows antiphase features between both the bihemispheric extratropics (Fig. 2b). In particular, the synchronous IHO–surface pressure correlation coefficients are positive (negative) in the NH (SH), with remarkable correlations dominantly at the bihemispheric extratropics. The perceptible positive correlation regions are largely in middle–western Eurasia, northern North America and the Arctic Ocean, in comparison to the latitudinal bands in 60°–90°S that have significant negative correlations generally. The significant positive correlation regions are also present in the middle and southern regions of Africa and South America and in the Northwest Pacific, while a large area of negative correlation is shown in the Southeast Pacific. As shown in the Appendix, the IHO indices and their correlation with SAP are highly consistent between NCEP1 and NCEP2 reanalysis data. Therefore, the following analysis will be based on NCEP1.

As shown in the regression coefficients of 850-hPa wind anomalies upon IHO (Fig. 2c), the IHO effect changes the surface pressure, which to a great extent determines the low-level winds. In particular, the positive pressure anomalies in the northern high latitudes decrease the meridional pressure gradient and thus decelerate the westerlies over the north of 60°N, while accelerated westerlies display over its SH counterpart. Furthermore, notable wave-train-like flow can be found in midlatitudes of both the SH and NH, indicating a potential interaction with stationary waves accompanied by IHO-associated large-scale airmass redistribution.

The above results show that the IHO indices are closely connected with the redistributed air mass at the extratropics in both hemispheres, and with the teleconnection between extratropical bihemispheric circulations. Therefore, the IHO may act as the bridge for the interaction of circulations in both hemispheres, which can be used to explain the seesaw feature of Fig. 2a.

3.2. *Linkage of IHO with AAO and AO*

AO and AAO are the leading modes of atmospheric

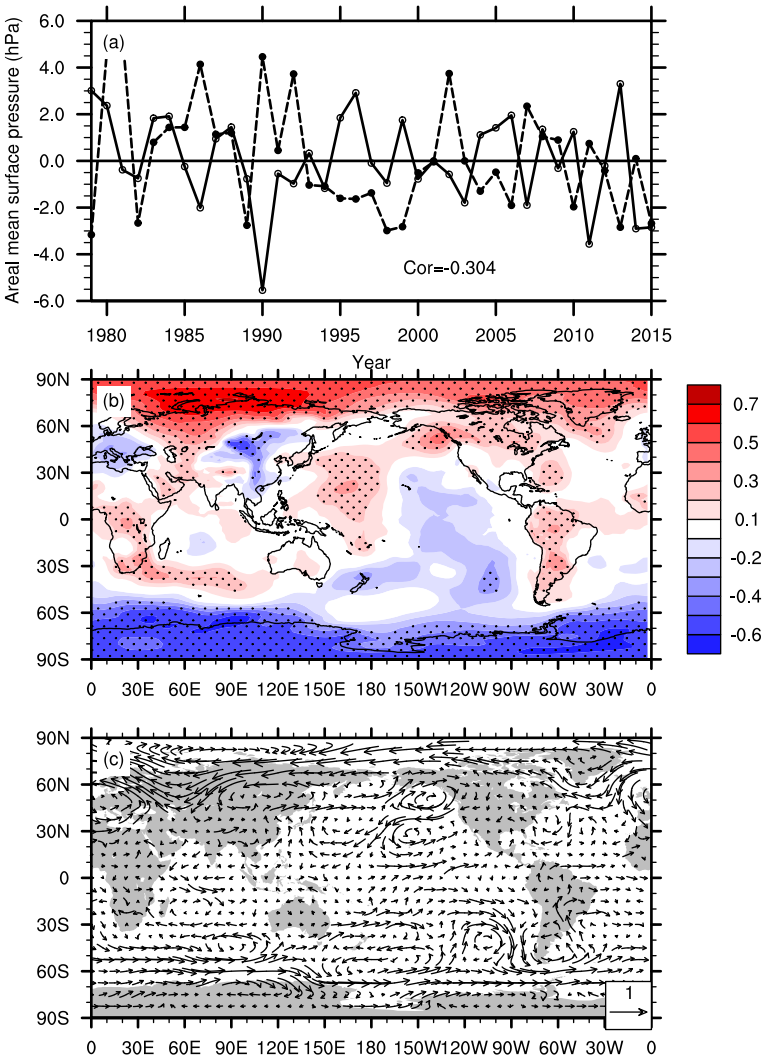

Fig. 2. (a) Spring area-weighted mean surface pressure over the Arctic (solid line) and Antarctic (dashed line) regions. (b, c) Correlation coefficients between IHO and (b) surface pressure and (c) anomalous wind (units: m s^{-1}) at 850 hPa regressed upon I_{IHO}. The dotted areas in (b) denote values exceeding the 90% confidence level.

Table 1. Correlation coefficients of IHO and regional mean SAP.

	NH_h & SH_h	IHO & NH_h	IHO & SH_h
DJF	0.19	0.10	0.59^{***}
MAM	-0.30^{*}	0.61^{***}	-0.62^{***}
JJA	–0.09	0.35^{**}	-0.61^{***}
SON	–0.05	0.33^{**}	-0.46^{***}

Note: Values with one, two and three superscript asterisks are statistically significant at the 0.1, 0.05 and 0.01 level, respectively, based on the *t*-test.

low-frequency variation at the extratropics for both hemispheres. Guan and Yamagata (2001) performed an EOF decomposition of zonally averaged surface pressure anomalies on a monthly basis, reaching AAO as the first mode, AO as the second mode, and IHO as the third mode, with variance contributions of 36.4%, 21.1% and 14.5%, respectively. These results indicated that the modes have a noticeable effect on the redistribution of atmospheric mass at a large scale. To reveal their interrelationships in spring, the correlation coefficients are computed between AAO and IHO, as well as AO and IHO, at the different levels given in Table 2, where the AAO calculation starts from 700 hPa because of the terrain. It is seen that AAO and AO are not closely related at any level except 700 hPa, which is in rough agreement with Baldwin and Thompson (2009), who showed no clear interaction happening between AAO and AO on a synchronous basis. However, there is a strong correlation between AAO/AO and IHO at these levels. In particular, IHO is positively correlated with AAO below 50 hPa, with correlation coefficients decreasing as a function of increasing height. In contrast, IHO and AO are negatively correlated from the troposphere to lower stratosphere. The above analysis demonstrates that the bihemispheric extratropical circulations are tied to IHO despite less inter-association between AAO and AO in the spring. In addition, the

Table 2. Correlation coefficients of IHO with AAO and AO, as well as AAO with AO, at all pressure levels.

Level (hPa)	IHO&AAO	IHO&AO	AAO&AO
1000	–	**−0.57**	–
925	–	**−0.57**	–
850	–	**−0.56**	–
700	**0.61**	**−0.53**	**−0.35**
600	**0.58**	**−0.52**	−0.31
500	**0.55**	**−0.51**	−0.26
400	**0.51**	**−0.49**	−0.19
300	**0.46**	**−0.48**	−0.14
250	**0.45**	**−0.48**	−0.11
200	**0.44**	**−0.45**	−0.08
150	**0.43**	**−0.39**	−0.02
100	**0.40**	**−0.33**	0.03
70	**0.37**	−0.29	0.05
50	**0.33**	−0.25	0.07
30	0.23	−0.19	0.12
20	0.17	−0.13	0.18
10	0.10	−0.02	0.27

Note: Bold numbers denote statistically significant values at the 0.05 level based on the *t*-test.

well-defined correlations between IHO and AAO/AO from the surface to the lower stratosphere show evidence for the associated troposphere–stratosphere atmospheric interaction.

3.3. *Zonal wind anomalies*

The redistribution of air masses is accomplished via wind transport, while the related pressure gradient change in turn modifies the wind field. To further study bihemispherical atmospheric linkage associated with IHO, we conduct regression analysis on zonal wind and meridional mass transportation based on the IHO index. The regressed anomalous zonal winds are characterized by a longitudinal teleconnection (Fig. 3a): a wavenumber 5 pattern is well organized in the middle to upper troposphere and lower stratosphere, and it extends meridionally from the Arctic to Antarctic regions. The maximum (minimum) values are centered at approximately 60°S (75°N) in the lower troposphere (stratosphere).

The connection between IHO and the wind field can also be shown by the pattern of anomalies of zonal mean meridional mass streamfunction (Ψ). The Ψ is calculated by a method of iteration using zonally averaged meridional winds (Qin et al., 2006). As depicted in Fig. 3b, the Ψ anomalies notably modulate the classic tri-cell circulations; regions of remarkable positive values are at the bihemispheric extratropics, centered at approximately 60°S and 65°N in the lower troposphere, in agreement with the large-value bands of zonal wind anomalies in Fig. 3a. This suggests that the atmospheric mass redistribution in association with IHO gives rise to the change in pressure gradients, thereby making the adjusted wind field associated with the meridional transport of air mass. In addition, the rising (sinking) branch of the low-latitude Hadley circulation cell corresponds to

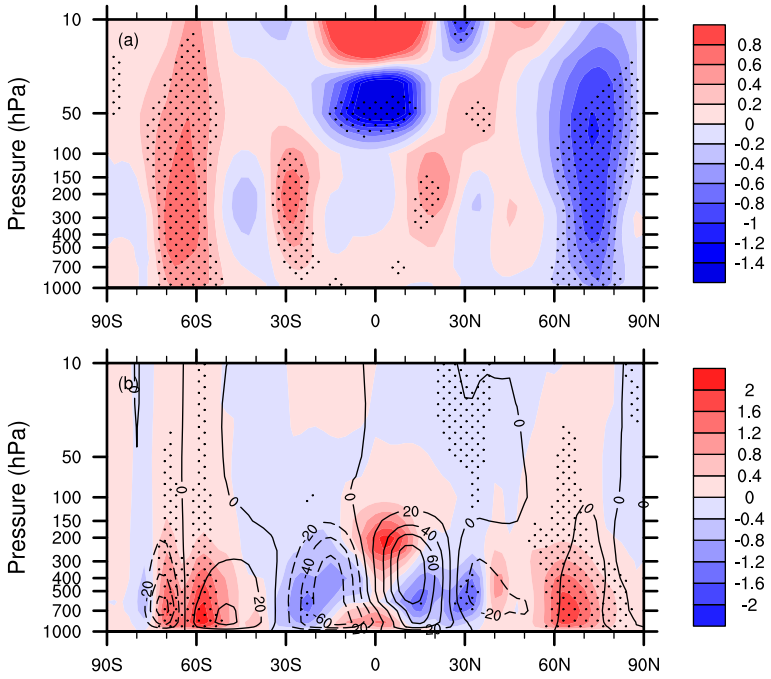

Fig. 3. Coefficients of (a) phase mean zonal wind anomalies (shaded; units: m s^{-1}) and (b) averaged meridional streamfunction anomalies (shaded; units: 10^9 kg s^{-1}) regressed upon normalized IHO, with the contours (spaced at 20 × 10^9 kg s^{-1}) in (b) denoting the climatology of mean meridional streamfunction. The dotted areas delineate the *F*-test significance values at 0.10.

the positive (negative) anomalies, indicating that when interhemispheric exchange is strengthened (i.e., the amplification of I_{IHO}), the related Hadley-cell transport is accelerated accordingly. Trenberth et al. (1998) showed that ENSO events play a driving role in extratropical circulation anomalies. Previous studies have also suggested that there is a close connection between tropical Pacific SST and extratropical atmospheric teleconnections (e.g., Alexander et al., 2002; Chen et al., 2014, 2015, 2017, 2018). As shown in Fig. 4, large areas of significant positive correlation coefficient between IHO and SST present in the middle and east of the tropical Pacific, potentially leading to an enhanced local Hadley circulation. SST anomalies and accompanying air–sea interaction over these areas may play an important role in triggering the atmospheric teleconnections between the northern high latitudes and its SH counterpart.

Figure 3 presents a marked meridional teleconnection pattern of winds between the middle–upper troposphere and lower stratosphere. This inspired us to further examine the zonal wind distributions at 250- and 500-hPa in Figs. 5a and b. The IHO-related 250- and 500-hPa zonal winds are clearly dominated by a meridional teleconnection. In particular, alternate positive–negative zonal bands are notably obvious in middle–eastern Eurasia, and the South/North Pacific and Atlantic. The meridional teleconnection of wind anomalies establishes the link between extratropical air masses in both hemispheres. These zonal wind anomalies are likely to produce effects on the midlatitude eddy–flow interplay, probably associated with overturning circulation and eddy dynamics (Chang, 1998; Seager et al., 2003), which may lead to an inter-association of tropical and extratropical air (Thompson and Lorenz, 2004).

3.4. *Anomalies of angular momentum*

The pattern of large-scale airmass anomalies is likely to change atmospheric angular momenta. Here, we address the maintenance mechanism of the interrelation between bihemispheric air at the extratropics through the changes in global angular momenta on the basis of its conservation, for which we use the coefficients of IHO regressed upon zonal mean wind $\bar{u}$ and surface pressure $\overline{p_s}$ to calculate associated omega angular momentum (m_Ω) and relative angular momentum (m_r) with Eq. (2). In Fig. 6, we see that the pattern of IHO-associated m_Ω anomalies exhibits a seesaw feature, with high values in the north and low values in the south, wherein the large values are mainly at the extratropics of both hemispheres, with the positive-value band(s) over 30°–90°N and negative-value center at approximately 60°S. According to Eq. (2), $m_\Omega(\varphi)$ is proportional to $\overline{p_s}\cos\varphi$, thereby demonstrating that the distribution of m_Ω anomalies is closely linked to the redistributed air mass from interhemispheric mass oscillation.

The numerical change in IHO-regressed m_r is greater in comparison to m_Ω, and the pattern of m_r anomalies exhibits a distinct meridional waveform. This resembles the pattern of $\bar{u}$ anomalies that are remotely related longitudinally on a global basis, showing that relative angular momenta play a role in maintaining the distribution of zonal wind anomalies. In view of the fact that the numerical change in m_r significantly exceeds that in m_Ω, the distribution of anomalies of IHO-related total angular momenta (m_Ω+m_r) approximates the pattern of m_r. Deserving of attention is the fact that the difference between (m_Ω+m_r) and m_r is pronounced at the extratropics (from 45° to the polar region in both hemispheres). Conservation of global angular momentum suggests that the effect of extratropical airmass anomalies on angular momentum is strengthened such that the combination of IHO-associated m_r and m_Ω anomalies can maintain the teleconnection of extratropical air masses in both hemispheres. On the other hand, AO- and AAO-related m_Ω and m_r present opposite spatial distributions primarily at bihemispheric middle–high latitudes—a result that is in agreement with

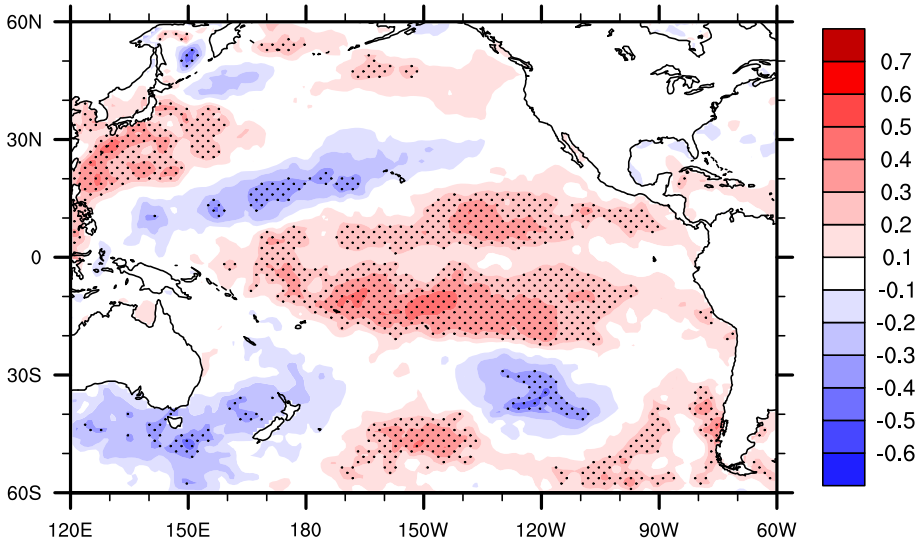

Fig. 4. Correlation coefficients between IHO and SST. Dotted areas denote values exceeding the 90% confidence level.

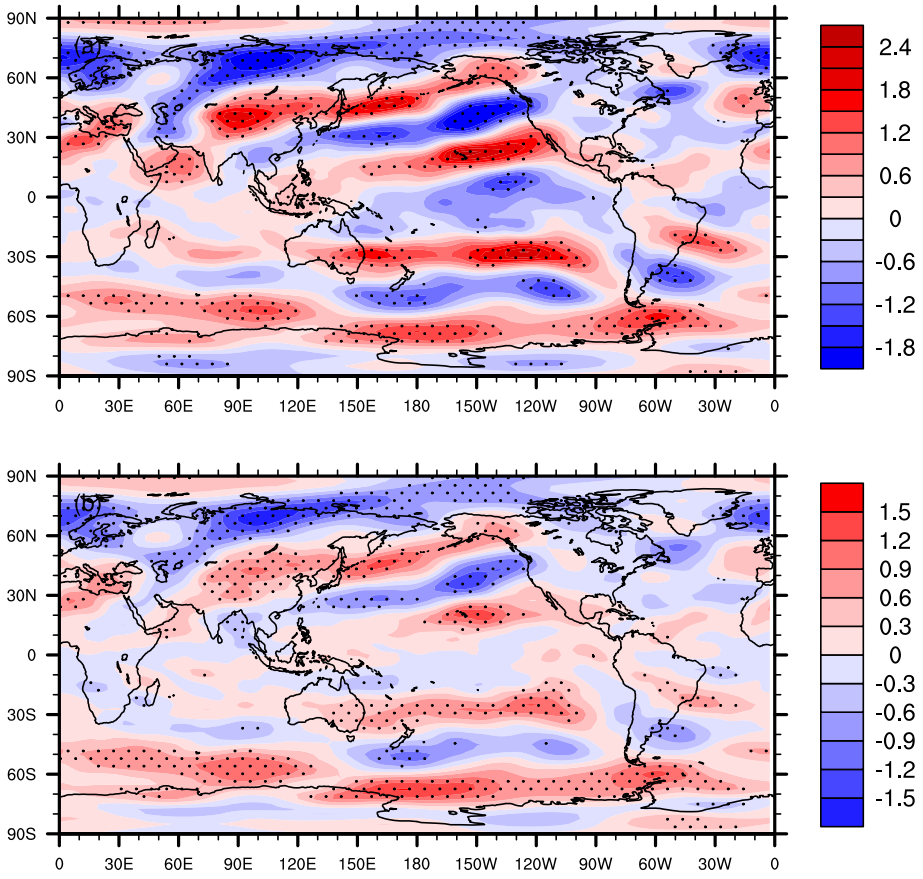

Fig. 5. Regression coefficients of (a) 250-hPa and (b) 500-hPa zonal wind anomalies (shaded; units: m s^{-1}) upon IHO indices, with dotted areas at the *F*-test confidence level of 90%.

that reported in von Storch (2000).

4. IHO from CMIP5

To verify the spatial pattern of IHO, we give the related results of the GFDL and UKMO models of CMIP5 in Fig. 7. Comparison shows that the pattern of correlation coefficients between IHO and surface pressure is close to that of Fig. 2b (Figs. 7a and c), including the prevalence of positive (negative) correlations in the NH (SH), and the large-value bands at the extratropics, except for some differences in the detailed distribution. In addition, the pattern of regression coefficients of zonal wind anomalies of these models upon IHO (Figs. 7b and d) exhibits strong alternate positive and negative banded anomalies from the Antarctic to Arctic region, in rough concert with the distribution of Fig. 3a. This configuration illustrates that the fundamental features of IHO-associated airmass oscillation between both hemispheres at the extratropics can be clearly reproduced in coupled climate models, showing that there is a rise of extratropical air mass in one hemisphere and a fall in the other, and this association may be produced via the meridional winds on a global basis.

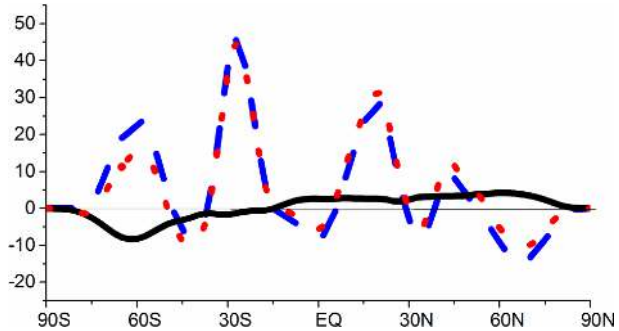

Fig. 6. IHO-regressed zonal mean m_Ω (black), m_r(blue) and (m_Ω+m_r) (red), in units of 10^{23} kg^2 m^2 s^{-1}.

5. Conclusions and remarks

This study uses spring NCEP reanalysis data from 1979–2017 to reveal a perceptible anticorrelation relationship between the hemispherically averaged atmospheric mass, thereby constructing IHO and showing the strength of interhemispheric exchange. The IHO-associated circulation anomalies are shown mainly by a pattern of opposite geopotential height anomalies at the extratropics from the troposphere to stratosphere between the hemispheres.

The spring IHO bears a positively (negatively) higher correlation to troposphere–stratosphere AAO (AO) signatures on a simultaneous basis, but the AAO–AO relation itself is not evident, which illustrates that IHO acts as a tie for the interrelation between bihemispheric circulations at the extratrop-

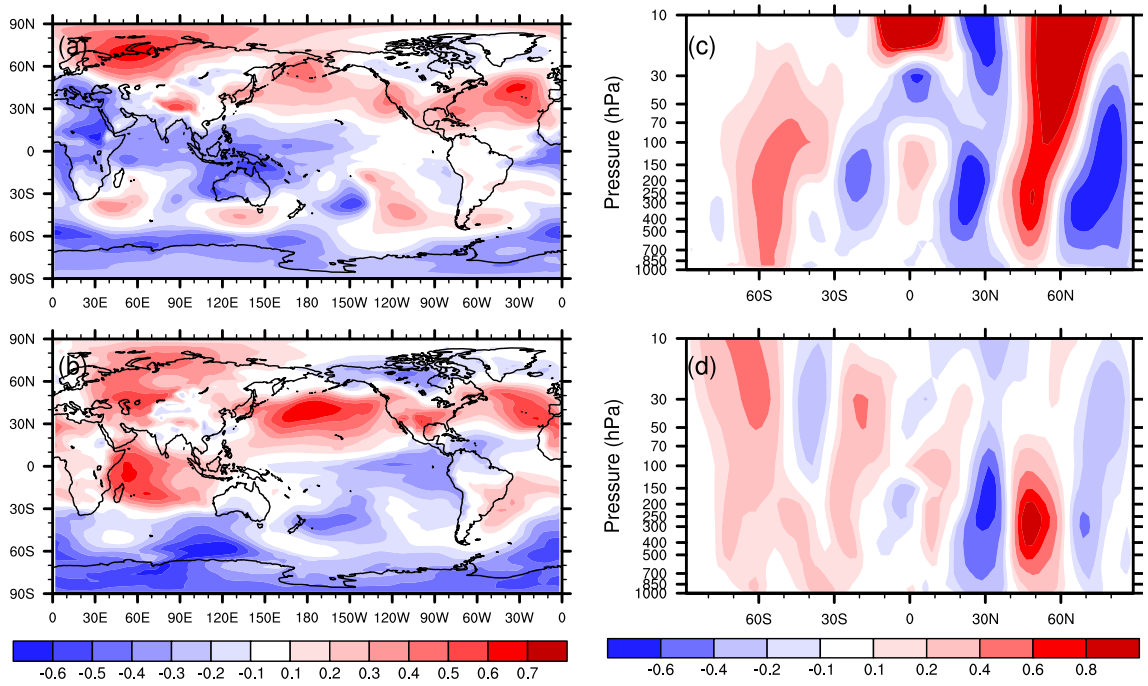

Fig. 7. (a, b) Correlation coefficients of IHO with surface pressure obtained from (a) GFDL and (b) UKMO (shaded). (c, d) Regression coefficients of IHO upon zonal wind for (c) GFDL and (d) UKMO (shaded; units: m s^{-1}).

ics, in relation to its interactions with the troposphere–stratosphere circulations at these latitudes.

Zonal wind anomalies from IHO regressions show a pronounced longitudinal teleconnection pattern in the middle–high troposphere to lower stratosphere, with belts of alternate positives and negatives extending from the Arctic to the Antarctic region, causing the adjustment of the mean meridional circulations and anomalies of meridional transport of air mass. In the spring months, IHO is bound up with the anomalies of angular momenta led by the atmosphere at these latitudes, and these anomalies trigger those of longitudinal waveforms of angular momentum, thereby associating them with anomalies of zonal winds and supporting bihemispheric teleconnection at the extratropics.

From the above analysis, IHO plays an import role in global-scale airmass redistribution and links closely with AO and AAO. However, it is worth noting that the IHO-associated global-integrated anomaly of the relative angular momentum is 3.64×10^{25} kg^2 m^2 s^{-1}, which is substantially larger than the omega angular momentum (0.17×10^{25} kg^2 m^2 s^{-1}). On the contrary, as reported by von Storch (2000), the size of the global-mean anomaly of the omega angular momentum induced by both is markedly larger than that of the relative angular momentum associated with the modeled AO and AAO. Smaller values of omega angular momentum anomalies in IHO results from mass conservation. The mass deficit at the southern high latitudes is a consequence of the excess at its NH counterpart.

This work is a preliminary study of the link between bihemispheric circulations at the extratropics, along with a possible approach to this association. In fact, the dynamic and thermal physics are extremely complicated for interactions between circulations at low, middle and higher latitudes, which require further simulation using air–sea coupled models. The use and verification of the GFDL and UKMO results lead to related IHO characteristics for future numerical simulations.

Acknowledgments. The authors would like to thank the Center of Atmospheric Data Service, Nanjing University of Information Science & Technology, under the Geoscience Department of the National Natural Science Foundation of China, and NOAA-CIRES Climate Diagnostics Center (http://www.cdc.noaa.gov/cdc/reanalysis/reanalysis.shtml) for providing data. This work is supported jointly by the National Basic Research Program of China (Grant No. 2015CB953904) and the National Natural Science Foundation of China (Grant Nos. 41975073, 41575081 and 41741005).

APPENDIX

Comparison of IHO in NCEP1 and NCEP2

We also constructed IHO indices and checked their correlation with SAP using NCEP2 reanalysis. As shown in Fig. A1, the variation of IHO time series and their relationship with SAP in both the northern and southern high latitudes shows substantial consistency between NCEP1 and NCEP2. Guan et al. (2010) also showed the similarity in IHO among NCEP1, ERA-40 and JRA. Therefore, the IHO linked with the seesaw variation between the interhemspheric air mass is a robust phenomenon in the reanalysis datasets.

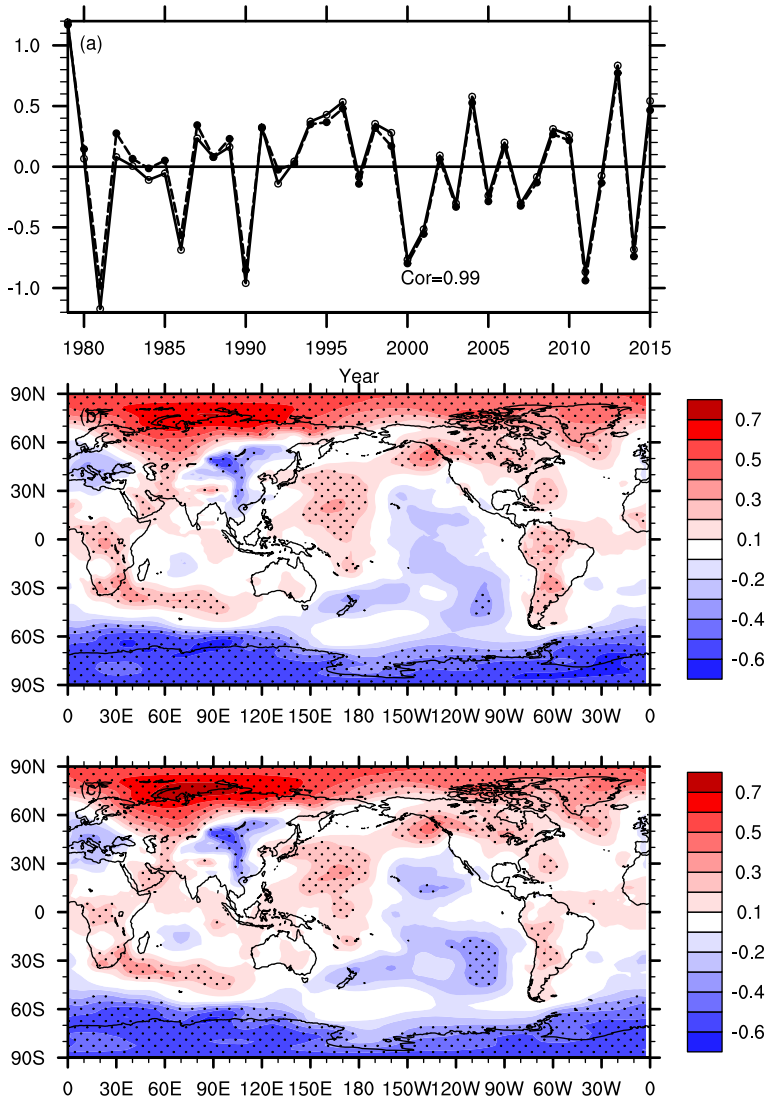

Fig. A1. (a) IHO index constructed by NCEP1 (solid line) and NCEP2 (dashed line). (b, c) Correlation coefficients between IHO and surface pressure in (b) NCEP1 and (c) NCEP2. The dotted areas in (b, c) denote values exceeding the 90% confidence level.

REFERENCES

Alexander, M. A., I. Bladé, M. Newman, J. R. Lanzante, N.-C. Lau, and J. D. Scott, 2002: The atmospheric bridge: The influence of ENSO teleconnections on air-sea interaction over the global oceans. *J. Climate*, **15**(16), 2205–2231, https://doi.org/10.1175/1520-0442(2002)015<2205:TABTIO>2.0.CO;2.

Baldwin, M. P., 2001: Annular modes in global daily surface pressure. *Geophys. Res. Lett.*, **28**, 4115–4118, https://doi.org/10.1029/2001GL013564.

Baldwin, M. P., and D. W. J. Thompson, 2009: A critical comparison of stratosphere-troposphere coupling indices. *Quart. J. Roy. Meteor. Soc.*, **135**, 1661–1672, https://doi.org/10.1002/qj.479.

Blewitt, G., D. Lavallée, P. Clarke, and K. Nurutdinov, 2001: A new global mode of earth deformation: Seasonal cycle detected. *Science*, **294**, 2342–2345, https://doi.org/10.1126/science.1065328.

Carrera, M. L., and J. R. Gyakum, 2003: Significant events of interhemispheric atmospheric mass exchange: Composite structure and evolution. *J. Climate*, **16**, 4061–4078, https://doi.org/10.1175/1520-0442(2003)016<4061:SEOIAM>2.0.CO;2.

Chang, E. K. M., 1998: Poleward-propagating angular momentum perturbations induced by zonally symmetric heat sources in the tropics. *J. Atmos. Sci.*, **55**, 2229–2248, https://doi.org/10.1175/1520-0469(1998)055<2229:PPAMPI>2.0.CO;2.

Chen, S. F., B. Yu, and W. Chen, 2014: An analysis on the physical process of the influence of AO on ENSO. *Climate Dyn.*, **42**, 973–989, https://doi.org/10.1007/s00382-012-1654-z.

Chen, S. F., B. Yu, and W. Chen, 2015: An interdecadal change in the influence of the spring Arctic Oscillation on the subsequent ENSO around the early 1970s. *Climate Dyn.*, **44**, 1109–1126, https://doi.org/10.1007/s00382-014-2152-2.

Chen, S. F., W. Chen, and B. Yu, 2017: The influence of boreal spring Arctic Oscillation on the subsequent winter ENSO in CMIP5 models. *Climate Dyn.*, **48**, 2949–2965, https://doi.org/10.1007/s00382-016-3243-z.

Chen, S. F., R. G. Wu, and W. Chen, 2018: A strengthened impact of November Arctic oscillation on subsequent tropical Pacific sea surface temperature variation since the late-1970s. *Climate Dyn.*, **51**, 511–529, https://doi.org/10.1007/s00382-017-3937-x.

Chen, T.-C., J.-M. Chen, S. Schubert, and L. L. Takacs, 1997: Seasonal variation of global surface pressure and water vapor. *Tellus A: Dynamic Meteorology and Oceanography*, **49**, 613–621, https://doi.org/10.3402/tellusa.v49i5.14825.

Christy, J. R., K. E. Trenberth, and J. R. Anderson, 1989: Large-scale redistributions of atmospheric mass. *J. Climate*, **2**, 137–148, https://doi.org/10.1175/1520-0442(1989)002<0137:LSROAM>2.0.CO;2.

Gong, D. Y., and S. W. Wang, 1999: Definition of Antarctic oscillation index. *Geophys. Res. Lett.*, **26**, 459–462, https://doi.org/10.1029/1999GL900003.

Guan, Z. Y., and T. Yamagata, 2001: Interhemispheric oscillations in the surface air pressure field. *Geophys. Res. Lett.*, **28**, 263–266, https://doi.org/10.1029/2000GL011563.

Guan, Z. Y., C. H. Lu, S. L. Mei, and J. Cong, 2010: Seasonality of interannual inter-hemispheric oscillations over the past five decades. *Adv. Atmos. Sci.*, **27**, 1043–1050, https://doi.org/10.1007/s00376-009-9126-z.

Kalnay, E., and Coauthors, 1996: The NCEP/NCAR 40-year reanalysis project. *Bull. Amer. Meteor. Soc.*, **77**, 437–472, https://doi.org/10.1175/1520-0477(1996)077<0437:TNYRP>2.0.CO;2.

Lu, C. H., and Z. Y. Guan, 2009: On the interannual variation in spring atmospheric inter-hemispheric oscillation linked to synchronous climate in China. *Progress in Natural Science*, **19**, 1125–1131, https://doi.org/10.1016/j.pnsc.2009.01.006.

Lu, C. H., Z. Y. Guan, S. L. Mei, and Y. J. Qin, 2008: The seasonal cycle of interhemispheric oscillations in mass field of the global atmosphere. *Chinese Science Bulletin*, **53**(20), 3226–3234, https://doi.org/10.1007/s11434-008-0316-3.

Namias, J., 1963: Large-scale air-sea interactions over the North Pacific from summer 1962 through the subsequent winter. *J. Geophys. Res.*, **68**, 6171–6186, https://doi.org/10.1029/JZ068i022p06171.

Nicholson, S. E., and D. Entekhabi, 1986: The quasi-periodic behavior of rainfall variability in Africa and its relationship to the southern oscillation. *Arch. Met. Geoph. Biocl. Series A*, **34**, 311–348, https://doi.org/10.1007/BF02257765.

Newell, R. E., D. G. Vincent, and J. W. Kidson, 1969: Interhemispheric mass exchange from meteorological and trace substance observations. *Tellus*, **21**, 641–647, https://doi.org/10.3402/tellusa.v21i5.10114.

Qin, Y. J., P. X. Wang, Z. Y. Guan, and Y. Yue, 2006: Comparison of the Hadley cells calculated from two reanalysis data sets. *Chinese Science Bulletin*, **51**, 1741–1746, https://doi.org/10.1007/s11434-006-2030-3.

Seager, R., N. Harnik, Y. Kushnir, W. Robinson, and J. Miller, 2003: Mechanisms of hemispherically symmetric climate variability. *J. Climate*, **16**, 2960–2978, https://doi.org/10.1175/1520-0442(2003)016<2960:MOHSCV>2.0.CO;2.

Thompson, D. W. J., and J. M. Wallace, 1998: The Arctic oscillation signature in the wintertime geopotential height and temperature fields. *Geophys. Res. Lett.*, **25**, 1297–1300, https://doi.org/10.1029/98GL00950.

Thompson, D. W. J., and D. J. Lorenz, 2004: The signature of the annular modes in the tropical troposphere. *J. Climate*, **17**, 4330–4342, https://doi.org/10.1175/3193.1.

Trenberth, K. E., 1976: Spatial and temporal variations of the Southern Oscillation. *Quart. J. Roy. Meteor. Soci.*, **102**, 639–653, https://doi.org/10.1002/qj.49710243310.

Trenberth, K. E., G. W. Branstator, D. Karoly, A. Kumar, N.-C. Lau, and C. Ropelewski, 1998: Progress during TOGA in understanding and modeling global teleconnections associated with tropical sea surface temperatures. *J. Geophys. Res.*, **103**, 14 291–14 324, https://doi.org/10.1029/97JC01444.

von Storch, J. S., 2000: Angular momenta of the Antarctic and the Arctic oscillations. *J. Climate*, **13**, 681–685, https://doi.org/10.1175/1520-0442(2000)013<0681:AMOTAA>2.0.CO;2.

Walker, G. T., 1924: Correlations in seasonal variations of weather IX. *Mem. Ind. Meteor. Dept*, **24**, 275–332.